Journal of Luminescence 155 (2014) 95–100

Contents lists available at ScienceDirect

Journal of Luminescence

journal homepage: www.elsevier.com/locate/jlumin

Luminescence spectroscopy and energy level location of lanthanide ions doped in $La(PO_3)_3$

T. Shalapska [a,*], P. Dorenbos [b], A. Gektin [c], G. Stryganyuk [d], A. Voloshinovskii [e]

[a] Institute of Physics, University of Tartu, 142 Riia street, 51014 Tartu, Estonia
[b] Delft University of Technology, Faculty of Applied Sciences, Department RST/FAME, 15, Mekelweg, 2629 JB Delft, The Netherlands
[c] Institute for Scintillation Materials, NAS Ukraine, 60 Lenin avenue, 61001 Kharkiv, Ukraine
[d] Helmholtz Centre for Environment Research, 15 Permoserstr, 04318 Leipzig, Germany
[e] Ivan Franko National University of Lviv, 8 Kyryla i Mefodiya street, 79005 Lviv, Ukraine

ARTICLE INFO

Article history:
Received 13 February 2014
Received in revised form
12 June 2014
Accepted 16 June 2014
Available online 23 June 2014

Keywords:
Lanthanide luminescence
Phosphates
Level location
Electronic structure

ABSTRACT

The luminescence properties of Ce^{3+}, Pr^{3+}, Nd^{3+}, Sm^{3+}, Eu^{3+} and Tb^{3+} doped $La(PO_3)_3$ phosphate were studied by vacuum ultra-violet spectroscopy at 10 K which gives information on the energies of 4f–5d excitation and emission and charge transfer bands of the dopants. All data are consistent with available models and have been used to construct the vacuum referred binding energy scheme for all trivalent and all divalent lanthanides in $La(PO_3)_3$ phosphate.

1. Introduction

The inorganic compounds with general formula $Ln(PO_3)_3$ (Ln=La to Lu and Y) belong to the broader class of phosphate materials which have been extensively investigated because of a suitable absorption in the VUV region, a wide band gap together with a high chemical stability, and the relative simplicity of powder synthesis [1,2]. The Ce^{3+} luminescence in $Ce(PO_3)_3$ was studied by Ternane et al. [3], and in $Lu(PO_3)_3$ by Yuan et al. [4]. These materials are potential good phosphors, scintillators, and detectors for ionizing radiation. The scintillator properties of $Pr(PO_3)_3$ were studied by Jouini et al. [5]. The first investigation of Nd^{3+} luminescence in $La(PO_3)_3$ was reported by Jouini and co-authors in the framework of laser materials research [6]. The luminescence properties of Eu^{3+} and Tb^{3+} in $La(PO_3)_3$ and $Y(PO_3)_3$ as potential phosphors under VUV excitation have been discussed [2,7,8]. Much attention has been paid to the energy migration and transfer processes in Ln-based phosphate compounds [9–11].

$Ln(PO_3)_3$ (Ln=La to Lu and Y) is one of the complex phosphates, which can adopt two different crystal structures depending on the ionic radius of the Ln ion. $Ln(PO_3)_3$ (Ln=La to Gd) with a large radius of the Ln ion crystallizes in an orthorhombic structure with $C222_1$ space group, while those with small radius of Ln ion (Ln=Gd to Lu and Y) crystallize in the monoclinic crystal structure with $P2_1/c$ space group [12,13]. Recently, it was shown that the coordination environment of cationic sites can influence the luminescent properties of lanthanide ions in the two $Ln(PO_3)_3$ phosphate structures [8,12]. In particular, $La(PO_3)_3$ with the orthorhombic crystal structure has only one La-site with eight fold coordination that is available for the trivalent lanthanide ion dopant. Therefore, it is of interest to study the luminescence spectroscopy of lanthanide ions in $La(PO_3)_3$ and to establish where the lanthanide impurity energy levels are located. Information on the energy of electron transfer from the valence band to a trivalent lanthanide impurity forms a basis on which to construct a host referred binding energy diagram (HRBE) that presents the location of the $4f^n$ and $4f^{n-1}5d$ levels of all divalent and trivalent lanthanide ions relative to the top of the valence band [14,15]. Recently the chemical shift model was proposed that allows to convert a HRBE scheme into a vacuum referred binding energy scheme (VRBE) where all level energies are relative to that of an electron at rest in vacuum [16,17]. Such scheme provides a new method for the visualization of the location of the relevant lanthanide states with respect to each other and to the bands of the host compound. The first VRBE schemes were constructed for fluorides, aluminates, nitride compounds [18] and also already presented for some oxide materials [19–21].

In this work we present studies of the luminescence spectroscopy of lanthanides in $La(PO_3)_3$ under vacuum ultra-violet excitation. Data are used to construct the electronic structure scheme

* Corresponding author. Tel.: +372 7374766; fax: +372 7383033.
E-mail address: tetiana.shalapska@ut.ee (T. Shalapska).

http://dx.doi.org/10.1016/j.jlumin.2014.06.029
0022-2313/

with the binding energy of the electrons in the lanthanide impurity states and host band states. The spectroscopic information and the level scheme of $La(PO_3)_3$:Ln compound may then form a benchmark for the entire family of $Ln(PO_3)_3$ compounds (Ln=La to Gd). Additionally, we will compare the spectroscopy and the energy level scheme of $La(PO_3)_3$:Ln with the previous-studied system $LiYP_4O_{12}$:Ln [22] and other phosphate compounds.

2. Experimental details

The studies in this work were performed on powder samples of $La(PO_3)_3$:5 at% Ln (Ln=Ce, Pr, Nd, Sm, Eu and Tb) metaphosphate compounds prepared using the melt solution technique. For the synthesis of the phosphate, La_2O_3, CeO_2, Pr_2O_3, Nd_2O_3, Sm_2O_3, Eu_2O_3 and Tb_2O_3 oxide compounds together with $NH_4H_2PO_4$ were used as the starting materials. They were mixed and fired in quarts crucibles first at 300 °C for 24 h and then at 800 °C for 12 h. After cooling down to RT, the samples were washed and drained.

Measurements of luminescence excitation and emission spectra, decay kinetics within a 100 ns time-gate at 10 K, were performed at Deutsches Elektronen Synchotron (DESY, Hamburg) using synchrotron radiation from the DORIS III storage ring employing the SUPERLUMI experimental facility of HASYLAB [23]. A helium flow-type cryostat was used to stabilize the temperature at $T=10$ K. The emission in the UV visible range was recorded with a spectral resolution of 0.3–5.0 nm using a 0.3 m ARC Spectra Pro 308 monochromator-spectrograph in Czerny–Turner mounting equipped with 1200 or 300 groves/mm gratings and a Princeton Instruments CCD detector (1100 × 300 pixels) or a HAMAMATSU R6358P photomultiplier. The VUV emission spectra were recorded with 2 nm resolution using a 0.5 m Pouey-type monochromator equipped with a solar blind Hamamatsu R6836 photomultiplier. Luminescence excitation spectra were scanned within the 3.7–10 eV range with the resolution of 0.32 nm using the primary 2 m monochromator in 151 McPherson mounting (equipped with a Jobin Yvon holographic concave grating with Al+MgF_2 coating and 1200 groves/mm). The primary monochromator was calibrated with 0.005 nm accuracy using the $^1S_0 \rightarrow {}^3P_j$ absorption of atomic xenon and krypton gases as a reference. Luminescence excitation spectra were corrected for the incident photon flux by using Na-salycilate as a reference.

3. Experimental results

3.1. Ce^{3+} doping

The low temperature emission and excitation spectra of the $La(PO_3)_3$:Ce^{3+} metaphosphate are shown in Fig. 1. The emission spectra of the $La(PO_3)_3$:Ce^{3+} consist of the UV-emission bands peaking at 4.09 and 3.85 eV which are ascribed to the transitions from the lowest Ce^{3+} 5d excited state to the 4f ground state levels $^2F_{5/2}$ and $^2F_{7/2}$. The energy gap between the maxima coincides with the spin–orbit splitting of the Ce^{3+} ground state. The excitation spectrum of $La(PO_3)_3$:Ce^{3+} measured for the Ce^{3+}-related ($5d_1$–$^2F_{7/2}$) emission band ($E_{em}=3.82$ eV) reveals the presence of a structure typical for a Ce^{3+} ion in a low-symmetry crystal field with a dodecahedral coordination around the Ce^{3+} ion. Five excitation bands with the maxima at 4.27, 4.63 5.44, 6.11 and 6.43 eV are attributed to the transitions from the 4f ground state to the 5d excited states of a Ce^{3+} ion, which are split in the crystal field of the $La(PO_3)_3$ host lattice into $5d_1 \ldots 5d_5$ levels.

The values of the crystal field splitting, i.e., the energy difference between the highest-energy and the lowest-energy 5d bands ($\varepsilon_{cfs}=2.16$ eV) and the centroid shift, i.e., the average energy of the five 5d bands ($\varepsilon_c=0.974$ eV), are in a good agreement with expectation [24]. The peak due to the phosphate group excitations at 8.45 eV is weak, which indicates that the transfer efficiency of the excitation energy to Ce^{3+} is a rather poor. The decay time of Ce^{3+} emission upon the excitation in the region of the Ce^{3+} 4f–$5d^1$ excitation is exponential and can be characterized by the decay time of 14.8 ns (see inset Fig. 1).

3.2. Pr^{3+} doping

Fig. 2 presents the excitation and emission spectra of Pr^{3+} in $La(PO_3)_3$. The emission spectrum of $La(PO_3)_3$:Pr^{3+} reveals emission bands in the 6–2.8 eV spectral range typical for the $5d4f^1 \rightarrow 4f^2$ intracenter transitions in the Pr^{3+} ion. It is well established that the energy of the main 4f–5d excitation bands for Pr^{3+} can be predicted from the corresponding energies observed for Ce^{3+} by adding 1.56 eV ± 0.09 eV energy [15]. In Fig. 2, we therefore also presented the Ce^{3+} excitation spectrum from Fig. 1 shifted to 1.57 eV higher energy. A value of 1.57 eV provides a good agreement with the Pr excitation bands. One may recognize the $5d_{1-5}$ excitation bands of Ce^{3+} within the excitation spectrum for Pr^{3+} emission. The main Pr^{3+} excitation bands are accompanied by satellite bands at higher energy. For example the $5d_1$ and $5d_2$ Pr^{3+} excitation bands at 5.84 and 6.22 eV are accompanied by excitation bands at 6.03, 6.29, and 6.46 eV. These satellite bands are attributed to the coupling between the electron in the 5d orbital with the electron remaining in the 4f orbital. Similar structure of the excitation spectra of Pr^{3+} emission was observed for

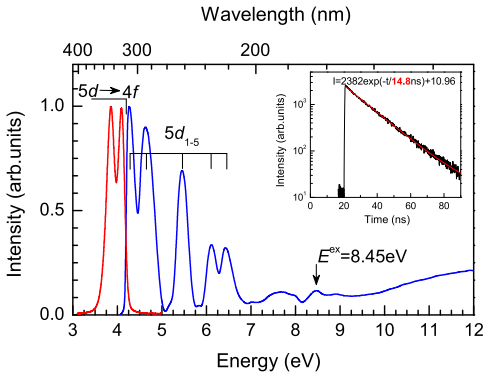

Fig. 1. The excitation spectrum of the 3.82 eV emission and the emission spectrum under the 5.46 eV excitation of Ce^{3+} in $La(PO_3)_3$ metaphosphate at 10 K. In the inset the low temperature decay curve of the Ce^{3+} luminescence for $La(PO_3)_3$:Ce^{3+} upon the excitation in the region of the Ce^{3+} 4f–$5d_1$ absorption ($E_{exc}=4.27$ eV and $E_{em}=3.82$ eV) is presented.

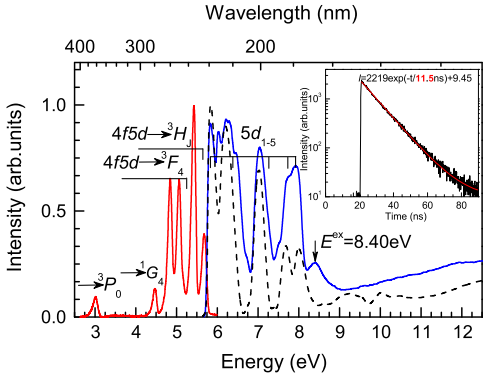

Fig. 2. The excitation spectrum of 5.39 eV emission and the emission spectrum under 7.04 eV excitation of Pr^{3+} in $La(PO_3)_3$ at $T=10$ K. The dashed curve shows the excitation spectrum of the Ce^{3+} emission shifted with 1.57 eV to higher energy. In the inset the decay curve of the Pr^{3+} luminescence for $La(PO_3)_3$:Pr^{3+} upon the excitation in the region of the Pr^{3+} 4f–5d absorption is presented at $T=10$ K.

YPO_4:Pr^{3+} [25] and $LiYP_4O_{12}$:Pr^{3+} [22]. The excitation bands peaking at 7.04, 7.7 and 7.92 eV correspond to the $5d_3$ $5d_4$ and $5d_5$ related excitation bands. The emission bands at 5.67, 5.43, 5.07, 4.84, and 4.47 eV are identified as emissions from the lowest 4f5d state to $^3H_4$, $^3H_5$, $^3H_6$, $^3F_2$, $^3F_{3,4}$, and $^1G_4$ states of Pr^{3+}, respectively. The emission band at 3.0 eV can be the spin allowed transition to the $^3P_0$ level. The Stokes shift between the $5d_1$ excitation and emission bands of $La(PO_3)_3$:Pr^{3+} is 0.17 eV. The maximum of the phosphate group excitation E^{ex} is 8.40 eV which is close to that observed for $La(PO_3)_3$:Ce^{3+}.

The decay curve of the Pr^{3+} 5d–4f luminescence in $La(PO_3)_3$ excited at 6.32 eV demonstrates a single-exponential behavior with the decay time $\tau = 11.5$ ns at $T = 10$ K, which is similar to the Pr^{3+} 5d–4f emission decay observed in other Pr-doped phosphates (11.8 ns for YPO_4 and 15.4 ns for $LuPO_4$, 13.4 ns for $LaPO_4$:Pr^{3+} [26], and 10.5 ns for $LiYP_4O_{12}$:Pr^{3+} [27]). The life time of the Pr^{3+} emission is a factor 1.3 shorter than that observed for Ce^{3+}. Usually, the photon cascade emission process in Pr^{3+}-activated compounds is only realized when the lowest crystal field split level of the Pr^{3+} $4f^15d^1$ configuration is located energetically above the $^1S_0$ state of the $4f^2$ configuration [28]. For Pr^{3+}-doped $La(PO_3)_3$ the relaxed lowest energy 4f–5d state is located below the $4f^2$ [$^1S_0$] state, and photon cascade emission from the $4f^2$ [$^1S_0$] therefore does not occur.

3.3. Nd^{3+} doping

Fig. 3 presents the excitation and emission spectra for Nd^{3+} in $La(PO_3)_3$. The lowest 5d state of Nd^{3+} is predicted at about 2.80 eV higher energy than that for Ce^{3+} [15]. In Fig. 3 the first four excitation bands observed for Ce^{3+} are shifted by 2.75 eV in energy in order to compare with the Nd^{3+} excitation bands. The bands in the Nd^{3+} excitation spectrum at 7.0 and 7.41 eV can be identified as the transition to the lowest energy $5d_1$ and $5d_2$ states. The emission to the $4f^3$[$^4I_{9/2}$] ground state is observed as a clear band at 6.87 eV yielding a Stokes shift of 0.13 eV. The emission to the $4f^3$[$^4I_{11/2}$] state is seen as a clear band at 6.65 eV. The emission to the $^4I_{13/2}$ and $^4I_{15/2}$ states is too weak to be observed. The emission bands around 5.46 eV and 4.74 eV are due to transitions to higher energy $4f^3$ states. The decay time of Nd^{3+} 5d–4f luminescence is 5.8 ns as shown in the inset of Fig. 3.

3.4. Sm^{3+} doping

The excitation and emission spectra of Sm^{3+}-doped $La(PO_3)_3$ are shown in Fig. 4. The sharp emission lines at 2.212, 2.083 and 1.933 eV are due to the $4f^5 \rightarrow 4f^5$ transitions starting from the $^4G_{5/2}$ to the $^6H_{5/2}$ ground state and higher $^6H_{7/2}$, and $^6H_{9/2}$ states, respectively. Usually, the first $4f^5$–$4f^45d$ excitation band of Sm^{3+} is at 3.22 eV higher energy than that for Ce^{3+} and it is then predicted at 7.49 eV. Therefore, the band at 7.46 eV is assigned to that excitation. The relatively narrow 4f–5d excitation bands are located on top of a much broader excitation band that we assign to the charge transfer (*CT*) band. The maximum of this *CT*-band is around 7.13 eV. The 4f–5d excitation features on a top of the broad underlying *CT*-band are very similar as in $LiYP_4O_{12}$:Sm^{3+}. According to data presented in Ref. [11], the decay time of Sm^{3+} luminescence ($^4G_{5/2} \rightarrow {}^6H_{9/2}$) in $La(PO_3)_3$ phosphate under excitation in the region of the ^4I_J level is exponential with a decay time 2.6 ms at 300 K.

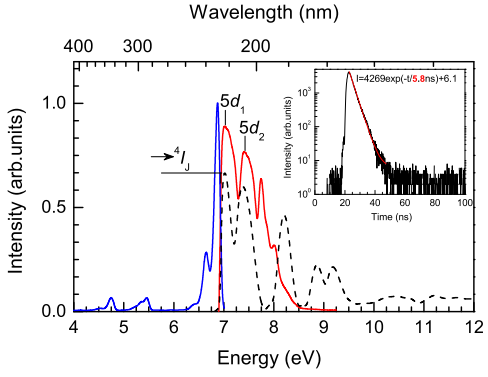

Fig. 3. The excitation spectrum of 6.84 eV emission and the emission spectrum under 7.12 eV excitation of Nd^{3+} in $La(PO_3)_3$ at 10 K. The dashed curve is part of the excitation spectrum of the Ce^{3+} emission shifted by 2.75 eV to higher energy. The inset presents the low temperature decay kinetics curve of Nd^{3+} luminescence in $La(PO_3)_3$ upon excitation at $E_{exc} = 6.81$ eV.

3.5. Eu^{3+} doping

Fig. 5 presents the excitation and emission spectra for Eu^{3+} in $La(PO_3)_3$. 5d–4f emission has never been observed with Eu^{3+} in any compound, and the emission spectrum shows only narrow intense $4f^6$–$4f^6$emission lines at 1.783, 1.9 (weak), 2.014, 2.084, 2.099 and 2.117 eV due to the $^5D_0 \rightarrow {}^7F_J$ ($J = 1$, 2, 3 and 4) radiative transitions. The excitation band to the lowest energy $4f^55d$ state is expected at 4.38 eV higher than that for Ce^{3+} yielding a predicted value of 8.65 eV which is the region of the phosphate group excitation band seen at $E^{ex} = 8.50$ eV. The strong and broad excitation starting at 5.80 eV is like for Sm^{3+} attributed to the *CT*-band, i.e., an electron is excited from the top of the valence band to Eu^{3+}. The maximum of the *CT*-band is at 5.84 eV. In addition, weak narrow excitation lines at 4.16 and 3.87 eV are

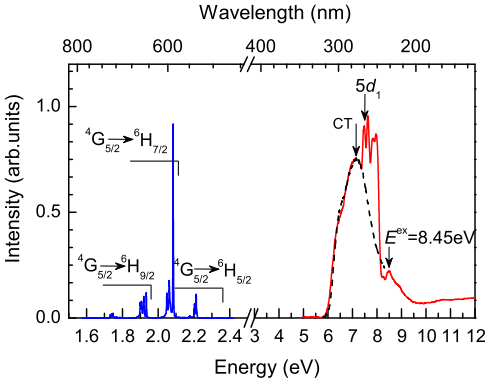

Fig. 4. The excitation spectrum of 2.07 eV emission and the emission spectrum under 7.13 eV excitation of Sm^{3+} in $La(PO_3)_3$ at 10 K. The dashed curve is part of the excitation spectrum of the Eu^{3+} emission shifted by 1.30 eV to higher energy.

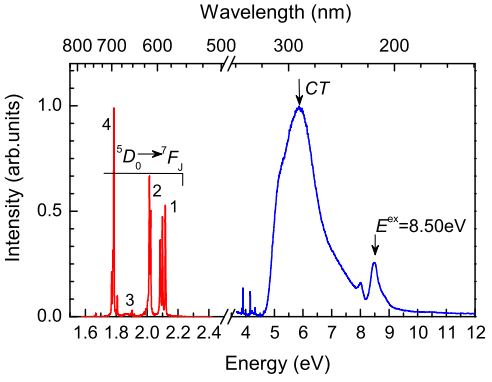

Fig. 5. The excitation spectrum of 2.11 eV emission and the emission spectrum under 7.09 eV excitation of Eu^{3+} in $La(PO_3)_3$ at 10 K.

observed that correspond to the $^7F_0 \rightarrow {}^5F_J$ and $^7F_0 \rightarrow {}^5H_J$ transitions of Eu^{3+}.

When the energy of *CT* to Eu^{3+} is known the energy of *CT* to any other trivalent lanthanide in the same compound can be predicted. That for Sm^{3+} is always at 1.25 eV higher energy than that for Eu^{3+}. To demonstrate this, the excitation spectra for Eu^{3+} have been shifted by 1.3 eV and shown in Fig. 4. It provides a prediction of the contribution from the Sm^{3+} *CT*-band to the excitation spectrum. The decay kinetics of the Eu^{3+} $^5D_0 \rightarrow {}^7F_2$ luminescence in $La(PO_3)_3$ were studied by Ternane et al. [3] and determined to be 3.85 ms at 300 K and 4.30 ms at 77 K.

3.6. Tb^{3+} doping

Fig. 6(a) shows the excitation and emission spectra of $La(PO_3)_3$:Tb^{3+}. In the emission spectra typical narrow emission lines are seen that correspond to the emissions from the $4f^8[^5D_3]$ and $4f^8[^5D_4]$ states to the lower energy ^7F_J multiples. The spin allowed transitions starting from the so-called low spin [LS] $5d_1$ state of Tb^{3+} are always found at 1.6 eV higher energy than those from the $5d_1$ state of Ce^{3+} [29]. In the case of $La(PO_3)_3$:Tb^{3+} the [LS] $5d_1$ excitation band is predicted at 5.93 eV which is in a good agreement with Fig. 6(a). The weak excitation band at 1.01 eV lower energy, 4.92 eV, is attributed to the first spin forbidden transitions to the high spin [HS] $5d_1$ state. The dashed line in Fig. 6 (b) shows the excitation spectrum of Ce^{3+}, which is shifted in energy by 1.64 eV. The location of the first four shifted Ce^{3+} excitation bands then agrees well with the observed bands of Tb^{3+}. The fifth excitation band of Tb^{3+} appearing as a shoulder band at 7.89 eV is at 0.16 eV lower energy than that predicted from the Ce^{3+} excitation spectrum. This suggests that the total crystal field splitting for Tb^{3+} is 0.16 eV smaller than that observed for Ce^{3+} and Pr^{3+} ions in this host lattice. The spin forbidden transition to [HS] $5d_3$ is predicted to coincide with the transition to the

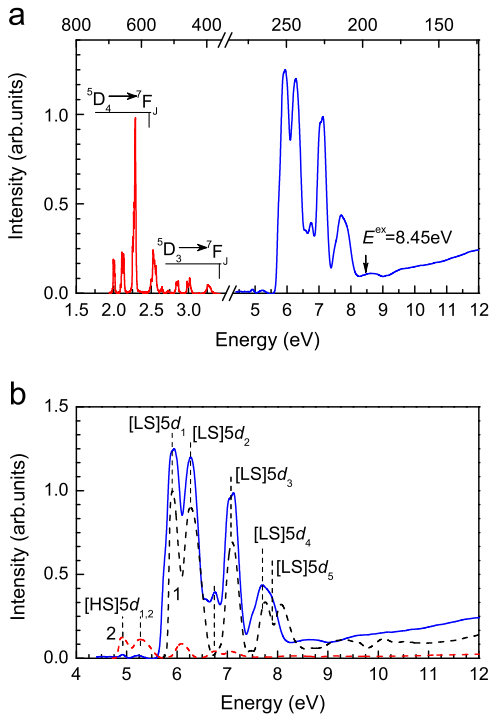

Fig. 6. (a) The excitation spectrum of 2.27 eV emission and the emission spectrum under 6.89 eV excitation of Tb^{3+} in $La(PO_3)_3$ at 10 K. (b) The excitation spectrum of 2.27 eV emission of Tb^{3+} together with the dashed curves (1) and (2) which are relevant parts of the excitation spectrum of Ce^{3+} emission shifted with 1.64 and 0.64 eV to higher energy, respectively.

[LS] $5d_2$. To illustrate this, the excitation spectrum of Ce^{3+} is shifted by 0.64 eV and shown as dashed curve 2 in Fig. 6(b). The excitation bands for Ce^{3+} then approximately reproduce the energies for the weak spin forbidden transitions to the [HS] $5d_i$ states of Tb^{3+}. Those to $5d_1$, $5d_2$, and $5d_4$ can then be identified. The decay kinetics of the $^5D_4 \rightarrow {}^7F_5$ transition of Tb^{3+} in $La(PO_3)_3$ under excitation in the region of the [LS] $5d_3$ absorption was studied by Wang et al. [2] and found to be about 4.47 ms at 300 K.

4. Discussion

Using the four crucial parameters as the redshift, the centroid shift, *CT*-energies, and exciton creation energies (see Table 1), the host referred binding energy (HRBE) and the vacuum referred binding energy (VRBE) scheme are constructed for $La(PO_3)_3$:Ln and presented in Fig. 7. The energy difference E_{VC} between the top of the valence band at E_V and the bottom of the conduction band at E_C is taken 8% larger than the exciton creation energy E^{ex}=8.45 eV in order to account for the estimated exciton binding energy [18]. E^{CT} defines the energy difference between E_V and the ground state energy $E_{4f}(7,2+,A)$ of Eu^{2+}. The ground state energy of Eu^{3+} is at $U(6,A)$ lower energy. $U(6,A)$ is known as the 4f-electron Coulomb repulsion energy and can be estimated from the centroid shift as in Ref. [30] where data for different inorganic compounds were presented. A value of 7.26 eV pertains to $La(PO_3)_3$ and then with the chemical shift model the absolute VRBE of the 4f ground state

Table 1
The experimental compound dependent input data for the shift model and the energies calculated therefrom; all energies are in eV.

	$La(PO_3)_3$	$LiYP_4O_{12}$
Exp. input		
$E^{ex}(A)$	8.45	8.63
$D(3+,A)$	1.85	1.93
$\varepsilon_c(1,3+,A)$	0.974	0.972
$E^{exch}(8,3+,A)$	1.02	0.97
$E^{CT}(6,3+,A)$	5.84	6.15
Model ouput		
$D(2+,A)$	0.95	1.0
$U(6,A)$	7.25	7.26
$E_{4f}(7,2+,A)$	−4.20	−4.20
$E_{5d}(7,2+,A)$	−0.88	−0.85
$E_{4f}(1,3+,A)$	−6.21	−6.23
$E_{5d}(1,3+,A)$	−1.94	−2.04
$E_V(A)$	−9.99	−10.4
$E_X(A)$	−1.59	−1.72
$E_C(A)$	−0.86	−1.03

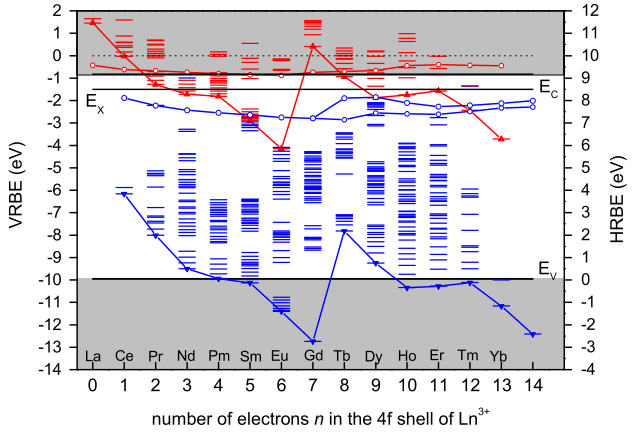

Fig. 7. The HRBE and VRBE scheme for the divalent and trivalent lanthanides in $La(PO_3)_3$.

Table 2
Observed and predicted energies for the first 4f–5d transition E_{fd} and for the *CT*-band energy E^{CT}. Values within brackets are for the first spin allowed 4f–5d transition; all energies are in eV.

Ln^{3+}	n	E_{df} $La(PO_3)_3$ obs.	E_{df} $La(PO_3)_3$ pred.	E_{CT} $La(PO_3)_3$ obs.	E_{CT} $La(PO_3)_3$ pred.
Ce	1	4.27	4.27		9.87
Pr	2	5.84	5.78		8.63
Nd	3	7.0	7.07		8.30
Pm	4	–	7.39		8.12
Sm	5	7.46	7.49	7.13	7.04
Eu	6	–	8.65	5.84	5.80
Gd	7	–	9.95		10.47
Tb	8	4.92 (5.93)	5.05		9.03
Dy	9	–	6.75		8.10
Ho	10	–	7.80		8.24
Er	11	–	7.70		8.42
Tm	12	–	7.65		7.57
Yb	13	–	8.85		6.29

energies for Eu^{2+} and Eu^{3+} are obtained which defines the left hand VRBE scale in Fig. 7.

The binding energies for divalent lanthanides other than Eu^{2+} are placed by using the $\Delta E(n+1,7,2+)$ parameters which give the characteristics upper double zigzag binding energy curve. $\Delta E(n,6,3+)$ parameters provide the lower double zigzag curve for the trivalent lanthanides: to this zigzag curve one may add the energy of the first spin allowed 4f–5d transitions by employing $E_{fd}(n,Q,A)=E_{fd}(n,Q,free)-D(Q,A)$. The first high spin [HS] 5d-level can be placed by multiplying $E^{exch}(n,3+,fluoride)$ values by 1.02 eV being the ratio $E^{exch}(n,3+,La(PO_3)_3)/E^{exch}(n,3+,fluoride)$ and subtracting that exchange splitting energy from the energy of the [LS] level. For indicating and determining the high spin [HS] 5d-states energies in $La(PO_3)_3$ we used the standardized notation and method from Ref. [30]. The VRBE scheme of $La(PO_3)_3$:Ln provides the information about the location of the lanthanide states and the host band states of $La(PO_3)_3$. In column 4 of Table 2 we compiled those predicted values using the most recent data from Ref. [30]. In column 3 the observed energies of 4f-5d transitions of Ln ions in $La(PO_3)_3$ are presented and the agreement with predicted energies is evident. The first spin-allowed transition was studied only for Tb^{3+} ion (shown within brackets). The *CT*-band energies of all lanthanides in $La(PO_3)_3$:Ln are also predicted and compiled in column 6 of Table 2. The energy of the observed *CT*-band for Sm^{3+} shown in column 5 agrees well with the predicted one. The conclusion at this stage is that there is a good agreement between the prediction from the VRBE schemes and the experimental data for $La(PO_3)_3$:Ln.

For comparison we show the VRBE energy scheme for $LiYP_4O_{12}$:Ln in Fig. 8. The values of $U(6,A)$ for $La(PO_3)_3$:Ln and $LiYP_4O_{12}$:Ln are about the same. All 4f-related binding energies in Fig. 7 are then also at about the same absolute energies as in Fig. 8. The main difference between the two schemes is in the binding energy of the host bands and differences in the redshift that affect the absolute $5d_i$-level locations. The valence band energy rises from -9.99 eV for $La(PO_3)_3$ to -10.40 eV for $LiYP_4O_{12}$; but the conduction band energy lowers from -0.86 eV to -1.03 eV, respectively. The anion coordination around lanthanum in $La(PO_3)_3$ is eightfold in the form of a dodecahedron with point symmetry C_2 like in $LiYP_4O_{12}$. The average La–O bond length is 253 pm [24] which is longer than the 239 pm in $LiYP_4O_{12}$.

The first VRBE scheme for YPO_4:Ln was presented in Ref. [16] and for other $REPO_4$:Ln (RE=La, Gd, Y, Lu, Sc) in Ref. [19]. In order to compare the level locations of the lanthanide states in different types of phosphate compounds the so-called stacked band structure diagram in Fig. 9 has been constructed. It compares the vacuum referred binding energy of the valence and conduction

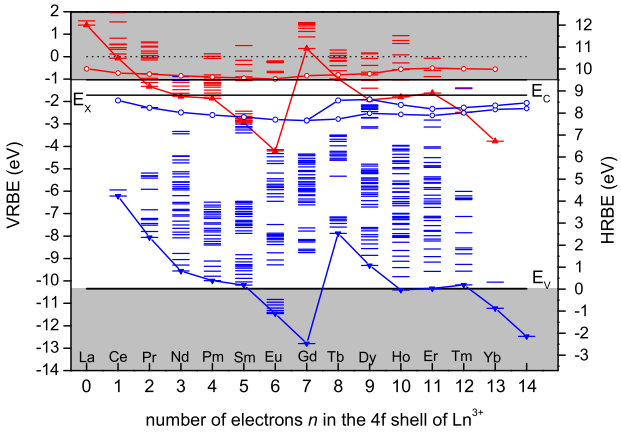

Fig. 8. The HRBE and VRBE scheme for the divalent and trivalent lanthanides in $LiYP_4O_{12}$.

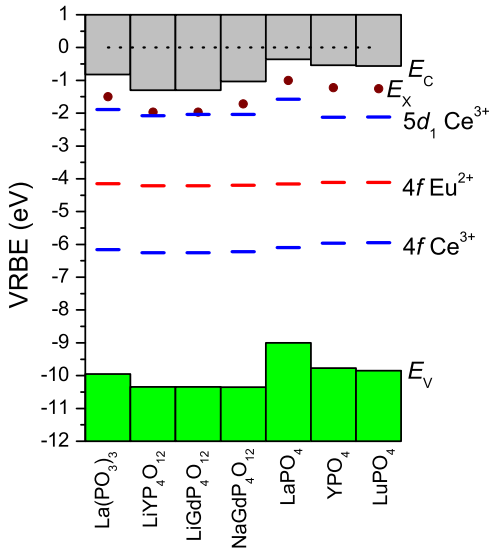

Fig. 9. Binding energy scheme showing the Ce^{3+} and Eu^{2+} 4f ground state levels and lowest energy Ce^{3+} $5d_1$ together with the energy E_V at the top of the valence band and E_C at the bottom of the conduction band. The solid data symbol shows the binding energy E_X of the electron in the host exciton state.

bands of various phosphate compounds together with the ground state of Ce^{3+} and Eu^{2+}, the first 5d-state of Ce^{3+} and the electron binding energy E_X in the exciton state ($E_X \equiv E_V + E^{ex}$). The data needed to construct the scheme are listed in Table 3.

The stacked scheme shows that the most important changes in the electronic scheme are due to changes in the valence band and the conduction band binding energy of the host compound. The impurity level ground state binding energies are fairly constant. Of particular interest for the temperature stability of the 5d–4f emission of Ce^{3+} is the energy difference E_{dC} between the $5d_1$ Ce level and the conduction and bottom. The values are listed in Table 3. Smallest E_{dC} is observed for $LaPO_4$ where the lowest temperature stability of Ce^{3+} 5d–4f emission is expected. $ALnP_4O_{12}$ (A=Li, Na) hosts will then provide better temperature stability due to an E_{dC} value above 1 eV which is twice larger than for $LnPO_4$ (Ln=La, Y and Lu) orthophosphates. The studied $La(PO_3)_3$ host shows $E_{dC}=0.86$ eV which is rather close to the $ALnP_4O_{12}$ hosts and which makes Ln doped $La(PO_3)_3$ compounds rather promising with respect to temperature stability of Ce^{3+} 5d–4f emission. Furthermore, it has a single crystallographic site of Ln ions and relatively simple single phase synthesis.

Table 3
Experimental data on the exciton creation energy E^{ex}(A) at the temperature near 10 K in the phosphate compounds and the results on E_V(A) and E_{dc}(A) from this work; all energies are in eV.

Compound	E^{ex}(A)	E_V(A)	E_{dC}(A)	Ref.
YPO_4	8.55	−9.77	−0.54	[19]
$LaPO_4$	8.0	−9.00	−0.36	[19]
$LuPO_4$	8.60	−9.85	−0.56	[19]
$La(PO_3)_3$	8.45	−9.99	−0.86	This work
$LiYP_4O_{12}$	8.63	−10.4	−1.03	[22]
$LiGdP_4O_{12}$	8.45	−10.4	−1.30	[31]
$NaGdP_4O_{12}$	8.30	−10.3	−1.30	[31]

5. Concluding remarks

The luminescence spectroscopy of Ce^{3+}, Pr^{3+}, Nd^{3+}, Sm^{3+}, Eu^{3+} and Tb^{3+} in $La(PO_3)_3$ has been studied upon vacuum ultraviolet excitation at $T=10$ K. The vacuum referred binding energy scheme for all trivalent and all divalent lanthanides in $La(PO_3)_3$ has been constructed and the predictions energies of the 4f–5d transition of lanthanide ions agree with the experiment. The same applies for the predicted *CT*-band energies.

Acknowledgments

The work is supported by institutional research funding IUT (02–26) of the Estonian Ministry of Education and Research, Estonian Science Foundation Grant no 8678 and the 7th FP INCO.2010-6.1 Grant agreement no. 266531 (project acronym SUCCESS). T. Shalapska is grateful to the Marie Curie Actions Postdoctoral Research Grant no. 0057J.

The authors appreciate the support of HASYLAB (DESY, Hamburg) for the Superlumi experiments.

References

[1] S. Hachani, B. Moine, A. El-akrmi, M. Ferid, J. Lumin. 130 (2010) 1774.
[2] Yu Wang, D. Wang, J. Solid State Chem. 180 (2007) 3450.
[3] R. Ternane, M. Ferid, G. Panczer, M. Trabelsi-Ayadi, J. Phys. Chem. Solids 69 (2008) 1684.
[4] J.-L. Yuan, H. Zhang, J.-T. Zhao, H.-H. Chen, X.-X. Yang, G.-B. Zhang, Opt. Mater. 30 (2008) 1369.
[5] A. Jouini, J.C. Gâcon, M. Ferid, M. Trabelsi-Ayadi, Opt. Mater. 24 (2003) 175.
[6] A. Jouini, J.C. Gâcona, A. Brenier, M. Ferid, M. Trabelsi-Ayadi, J. Lumin. 99 (2002) 365.
[7] D. Wang, Y. Wang, Y. Shi, J. Lumin. 131 (2011) 1154.
[8] R. Ternanea, M. Ferid, G. Panczer, M. Trabelsi-Ayadi, G. Boulon, Opt. Mater. 27 (2005) 1832.
[9] H.S. Kiliaan, F.P. van Herwijnen, G. Blasse, J. Solid State Chem. 74 (1988) 39.
[10] M. Buijs, G. Blasse, J. Lumin. 39 (1988) 323.
[11] S. Hachani, B. Moine, A. El-akrmi, M. Ferid, J. Lumin. 130 (2010) 1774.
[12] H.A. Höppe, K. Kazmierczak, S. Kacprzak, I. Schellenberg, R. Pottgen, Dalton Trans. 40 (2011) 9971.
[13] D. Wang, Yu Wang, Y. Shi, J. Lumin. 131 (2011) 1154.
[14] P. Dorenbos, J. Lumin. 91 (2000) 155.
[15] P. Dorenbos, J. Lumin. 111 (2005) 89.
[16] P. Dorenbos, Phys. Rev. B 85 (2012) 165107.
[17] P. Dorenbos, ECS J. Solid State Sci. Technol. 2 (2013) R3001.
[18] P. Dorenbos, Phys. Rev. B 87 (2013) 035118.
[19] P. Dorenbos, J. Phys.: Condens. Matter 25 (2013) 225501.
[20] P. Dorenbos, J. Lumin. 134 (2013) 310.
[21] P. Dorenbos, J. Lumin 136 (2013) 122.
[22] P. Dorenbos, T. Shalapska, G. Stryganyuk, A. Gektin, A. Voloshinovskii, J. Lumin. 131 (2011) 633.
[23] G. Zimmerer, Radiat. Meas. 42 (2007) 859.
[24] P. Dorenbos, Phys. Rev. B 64 (2001) 125117.
[25] L. van Pieterson, M.F. Reid, R.T. Wegh, S. Soverna, A. Meijerink, Phys. Rev. B 65 (2002) 045113.
[26] A. Zych, M. de Lange, C. de Mello Donega, A. Meijerink, J. Appl. Phys. 112 (2012) 013536.
[27] T. Shalapska, G. Stryganyuk, D. Trots, Yu Romanuchun, A. Gektin, A. Voloshinovskii, P. Dorenbos, J. Phys. D: Appl. Phys. 43 (2010) 405404.
[28] A.M. Svirastava, A.A. Setlur, H.A. Comanzo, W.W. Beers, U. Happek, P. Schmidt, Opt. Mater. 33 (2011) 292.
[29] P. Dorenbos, J. Phys.: Condens. Matter 15 (2003) 6249.
[30] P. Dorenbos, J. Lumin. 135 (2013) 93.
[31] T. Shalapska, G. Stryganyuk, P. Demchenko, A. Voloshinovskii, P. Dorenbos, J. Phys.: Condens. Matter 21 (44) (2009) 445901.